ORIGINAL RESEARCH

A Stable EEG Epilepsy Network Spans From Infraslow to Ripple and From Interictal to Ictus

Sushma Ghimire,* Mukesh Dhamala,*‡§ and Charles M. Epstein‖

Departments of *Physics and Astronomy and ‡Mathematics and Statistics, Georgia State University, Atlanta, Georgia, U.S.A.; §Neuroscience Institute, Georgia State University, Atlanta, Georgia, U.S.A.; and ‖Department of Neurology, Emory University School of Medicine, Atlanta, Georgia, U.S.A.

Purpose: To characterize the epilepsy network as reflected in intracranial electroencephalography (iEEG) across the full spectrum of iEEG frequencies and different phases of epilepsy, using a single, conceptually straightforward mathematical measure.

Methods: The authors applied the spectral Granger causality techniques to intracranial electroencephalography recordings and computed contact-by-contact inward, outward, and total causal flow across frequencies and seizure phases in a selected group of three patients with well-defined, nonlesional seizure foci and prolonged responses to invasive procedures. One seizure and one interictal sample were analyzed per subject.

Results: A prominent intracranial electroencephalography network was identified by Granger causality at both high and low frequencies. This network persists during the preictal and interictal phases of epilepsy and closely matches the visible seizure onset. The causal inflow network corresponded to seizure onset electrode contacts in 8 of 12 conditions, including ripple, infraslow, preictal, and interictal phases of epilepsy. Its most striking feature is the consistent dominance of causal inflow rather than outflow in the vicinity of the seizure onset zone.

Conclusions: Findings of this study indicate that a stable intracranial electroencephalography epilepsy network persists, and it can be characterized by a single Granger causality measure from infraslow to ripple frequencies and from the interictal to the immediate preictal phases of epilepsy.

Key Words: Infraslow EEG, Ripple frequency, Preictal, Interictal, Granger causality, Seizure propagation network.

(J Clin Neurophysiol 2022;00: 1–6)

Epilepsy is now recognized as a network disorder, even in patients for whom the seizure onset zone (SOZ) is highly localized and long-term remission can be obtained by focal ablations. Identifying SOZs and propagation networks in the brain has immediate importance not only for tissue resections or ablations but also for other treatments such as stimulation and focal gene therapy. A wide variety of mathematical techniques have been directed toward delineating the epilepsy network as it is reflected in intracranial electroencephalography (iEEG), including the visible ictus, the immediate preictal period, and the interictal phase of epilepsy. These analyses have involved the classic range of visual EEG, gamma frequencies, high-frequency oscillations above gamma (ripple), and undifferentiated broadband recordings.[1–4] Although several series have demonstrated significant predictive value for the SOZ, the results are difficult to compare among different techniques and may omit the clinically important distinction between patients with and without corresponding structural lesions on imaging. Thus, the computational results are promising but challenging to synthesize into a coherent picture. And despite indications that infraslow activity well below the classic visual range may also carry important information about the SOZ and epileptic network,[5–10] very low frequencies have generally been omitted from quantitative analysis.

Several variants of Granger causality (GC)[11] have been used separately to identify the SOZ at classic and ripple frequencies, during both the preictal and the interictal phases of epilepsy.[4,12–15] Extending the application of a frequency-dependent GC measure to the infraslow band and across frequencies and states in a select group of patients, we describe here a striking consistency among the iEEG networks identified by GC at both ripple and infraslow EEG frequencies. This network persists during the preictal and interictal phases of epilepsy and matches the visible seizure onset.

METHODS

Patient Selection

Data were analyzed under protocols approved by the Institutional Review Board of Emory University School of Medicine. Patients A, B, and C were chosen retrospectively based on meeting the following criteria: an established history of medication-refractory epilepsy; absence of obvious anatomic lesions on 3-Tesla MRI; a strong, sustained clinical response after a focal invasive procedure; and identification by the treating clinicians of visible seizure onset confined to one or two adjacent seizure onset contacts (SOCs) using contemporary iEEG criteria[16–18]—or, in the case of a patient with bilateral independent onsets, both seizure onsets could be so defined.

The authors have no funding or conflicts of interest to disclose.

M. Dhamala and C. M. Epstein are joint corresponding authors.

This research was supported by Georgia State University's Brains and Behavior Program to S. Ghimire and M. Dhamala, and by research funding through Emory University to C. M. Epstein.

Address correspondence and reprint requests to Charles M. Epstein, MD, Department of Neurology, Emory University School of Medicine, 12 Executive Park Drive, Atlanta, GA 30329, U.S.A.; e-mail: charles.epstein@emory.edu.

ISSN: 0736-0258/22/0000-0001
DOI 10.1097/WNP.0000000000000971

Individual Patient Data are Given Below

Patient A elected responsive neural stimulation when the SOZ was localized to primary motor cortex and tissue ablation was assessed to carry a high risk of permanent neurologic deficit. Intracranial electroencephalography onset consisted of focal, rapidly evolving beta-gamma fast activity. Responsive neural stimulation has resulted in sustained, >90% reduction in clinically symptomatic seizures for 5 years, with no seizures reported during the past 3 years.

Patient B has been in complete remission (Engel 1A) for 6 years after laser ablation along the track of the seizure onset electrode, with the SOZ in anterior cingulate cortex. The iEEG onset pattern consisted of incrementing focal spikes riding on slow activity.

Patient C had no clinical seizures for 18 months (Engel 1A) after bilateral mesial temporal electrode explantation. The iEEG onset pattern consisted of focal gamma activity appearing on a sudden baseline shift. Over the subsequent 6 years, seizures have remained much milder and less frequent than before the implantation, and the patient has no longer considered surgical treatment. This case was assessed clinically as an instance of long-term remission related to implantation of intracranial electrodes,[19–21] in which marked and sustained improvement or remission can be considered confirmatory evidence for seizure origin at the site of implantation.

IEEG Recording

Patients underwent implantation of depth electrodes, subdural grids, and/or strip electrodes with spacing between contacts of 5 mm (Ad-Tech Medical, Racine, Oak Creek, WI), placed in various combinations according to the individual presurgical localization hypothesis. Intracranial electroencephalography recordings were made with an XLTEK system (Natus Medical, San Carlos, CA) using up to 128 contacts. Channels contaminated by artifact were eliminated by visual inspection. Validated samples were low pass filtered below 10 Hz and high pass filtered above 50 Hz for infraslow and high-frequency analyses, respectively. In our previous studies, the localizing information in the high-frequency range was found to be carried predominantly in the ripple band above 100 Hz,[4,12] so hereafter "high-frequency" and "ripple" will be used interchangeably. Initial oversampling and hardware anti-aliasing filters were followed by linear phase finite impulse filters (FIRs) with an order of 30, set to just below the Nyquist frequency for the final sampling rate of 500 or 1,000 Hz. Wideband European Data Format (EDF) data for analysis was downloaded with all digital filters "off."

Data Preprocessing and Analyses

The iEEG time-series data were filtered using forward and backward finite impulse filters in EEGLAB[22] and the temporal mean was removed. The pass band of finite impulse filters was 50 Hz to Nyquist frequency (half of the sampling frequency) for high-frequency (gamma plus ripple) analysis and that for infraslow oscillations was 0.01 to 0.1 Hz. Preictal data samples for high-frequency activity were taken for 10 to 30 seconds, ending 1 to 2 seconds before visible seizure onset. For low-frequency preictal activity, data samples were selected visually to correspond to the beginning and the end of a baseline shift that coincided or overlapped with the visible seizure onset. The 113-, 330-, and 1,550-second data samples were analyzed for interictal activity in patients A, B, and C, respectively. Figure 1 summarizes the data preprocessing and analysis steps.

Granger Causality Analysis

As in our previous studies,[4,12] we applied the spectral Granger causality analysis[23] to the filtered iEEG time-series of different seizure phases in each patient and examined the strengths and directions of causal relations among recording channels. The spectral Granger causality (GC) between two time series (1 and 2) is defined as[23,24]: $M_{2\to1}(f) = -ln(1-\frac{(\Sigma_{22}-\Sigma_{12}^2/\Sigma_{11})|H_{12}(f)|^2}{S_{11}(f)})$, where, $M_{2\to1}(f)$ is Granger causality at a frequency f from the 2nd to the 1st time series, Σ is the noise covariance matrix, and H(f) is the transfer function estimated by the multivariate vector autoregressive modeling of the time series data.

The spectral GC was computed using this definition and separated for the infraslow (0.01–0.1 Hz) and high (>50 Hz)

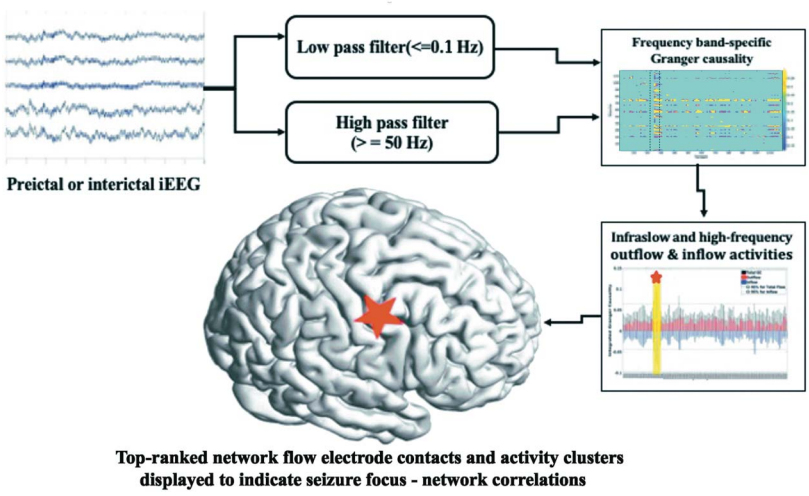

FIG. 1. Overview of the methods used in the present study. Preictal and interictal intracranial electroencephalography (iEEG) recordings were filtered to study high-frequency and infraslow frequency content. Frequency band-specific Granger causality measures were integrated to obtain total flow, inflow, and outflow. The causal flow activity was mapped and ranked across all recording electrode contacts. The star indicates the anatomic location of the electrode contacts at the SOZ and their corresponding position in the data histogram, also shown by the yellow outline.

frequencies. These infraslow and high-frequency Granger causality spectra were then integrated over the two frequency ranges (0.01–0.1 Hz, >50 Hz) to compute frequency band–specific Granger causality and to obtain matrices of causal relations among recording channels (nodes). Channel-specific outward, inward, and total causal flows were then computed from these band-specific Granger causality matrices. Outflow from *m*-node is a sum of the causal influences from that *m*-node to others divided by the number of rest of the nodes, i.e., $\text{outflow}_m = \frac{1}{(N-1)} \sum_{i=1}^{N} I_{m \to i}$, where $I_{m \to i}$ is a causal influence from *m*-node to *i*-node, the self-causality is zero, and N is the total number of nodes. Inflow was taken as the negative of the sum of the causal influences from the other nodes to the *m*-node divided by $N - 1$. We defined the total flow as the sum of the outflow and negative of the inflow. Here, we used the parametric approach to estimate Granger causality with a model order of 8 to 10 in all the analyses. The optimal model order was determined by examining differences in the power spectra from the nonparametric approach with the parametric approach at different model orders and selecting the model order that gave the lowest power difference as in our previous work.[4]

Statistical Significance

We computed (1) the GC threshold for overall statistical significance at $P < 10^{-6}$ using the random permutation method against the null model of no interdependence across channels of 1,000 shuffled time series segment samples, as in our previous studies[4,12] and (2) GC cluster confidence limits using the jackknife resampling method.[25]

In reviewing the significant GC values and causal flow patterns across the entire range of valid electrode contacts in each iEEG implant, we observed that regions of increased causal flow tended to cluster among adjacent contacts on individual electrodes, especially in regions around the seizure onset contacts. We therefore defined identification of the epilepsy network by one or more of the following criteria:

1. Increased GC inflow, outflow, or total flow at the SOC, ranking at the top 5% of all contacts, or
2. An identifiable cluster of increased causal flow including the SOC and ranking above the 95th percentile by jackknife resampling.[25]

Using jackknife resampling, we computed thresholds for clusters of six channels, removing and shuffling random samples of channels in each iteration to determine the distributions of total flow and inflow. Ninty-five percentage confidence interval thresholds computed from these distributions are shown in the figures by dotted and dashed lines. The cluster with the highest group average crossing the threshold line was selected as the most significant cluster.

RESULTS

Figure 2 shows causal flow matrices from patient A, in the contrasting conditions of interictal infraslow analysis and preictal high-frequency analysis. For both conditions, the dominant finding is a narrow zone of increased inflow that includes the site of visible seizure onset. Representative results for the complete sets of electrode implants are shown in Figs. 3 and 4 to illustrate most clearly the magnitude of causal flows and their relationships to the SOC. Figure 3, from patient C, involving the fewest electrodes, introduces the structure of these histograms, displaying outflow and total flow above the abscissa and inflow below it, and illustrates high-frequency activities during the interictal state. The patient had bilateral independent seizures recorded from mirror locations in the right and left hippocampus, with visible onset of types at the respective posterior hippocampal depth contacts 1 and 2. Strikingly, the contact pairs of visible onset rank 1, 2, 3, and 5 among all channels for both total flow and inflow. Figure 4A, from patient A, shows that the SOC ranks highest among 118 channels for causal inflow at infraslow frequencies during the interictal state. This contact is also contained in a cluster of inflow channels on the same electrode, which exceeds the 95% CI for inflow and is the highest ranking cluster overall. Figure 4B, from the same patient, shows that for preictal high frequencies, the SOC ranks 2nd of 118 contacts for inflow and total flow. The clusters of contacts surrounding it stands out significantly for both inflow and total flow as well. Figure 4C, from patient B, representing the preictal phase at infraslow frequency, shows that only the inflow cluster containing the SOC exceeds the 95% confidence interval. Here, the SOC ranks 5th of 123 channels but is exceeded only by its neighbors in that cluster.

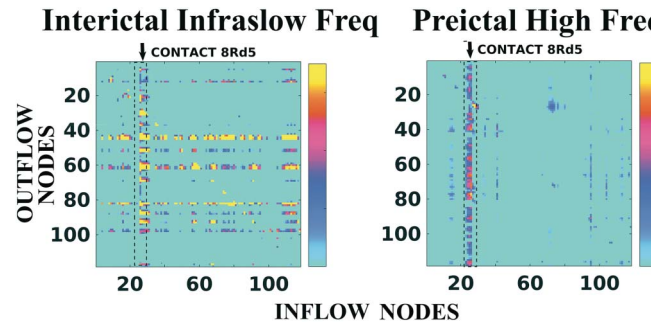

FIG. 2. Band-specific Granger causality for interictal infraslow frequencies and preictal high frequencies in a representative patient. The numbers in the axes denote the intracranial electroencephalography (iEEG) channels. Inflow and outflow are defined as the information flow toward and away from individual recording contacts. Both phases show the dominance of causal inflow at the region of the visible seizure onset (contact 8Rd5).

In summary, the SOC commonly rank very high for causal flow among the entire set of electrodes. Clusters of contacts containing the SOC might also stand out as significant for inflow or total flow.

Table 1 summarizes the correspondence of causal measures to the SOC. If, for patients with a single SOZ, the SOC rank among the top 5% for a given measure, this result is considered to be localizing and counted 1, otherwise it is counted 0. Thus, the values in the Table represent the number of patients for which that measure is able to localize the SOC. Causal outflow activity was never an independent predictor of the SOZ. As reported in the Table, the causal inflow measure corresponded to the SOC in

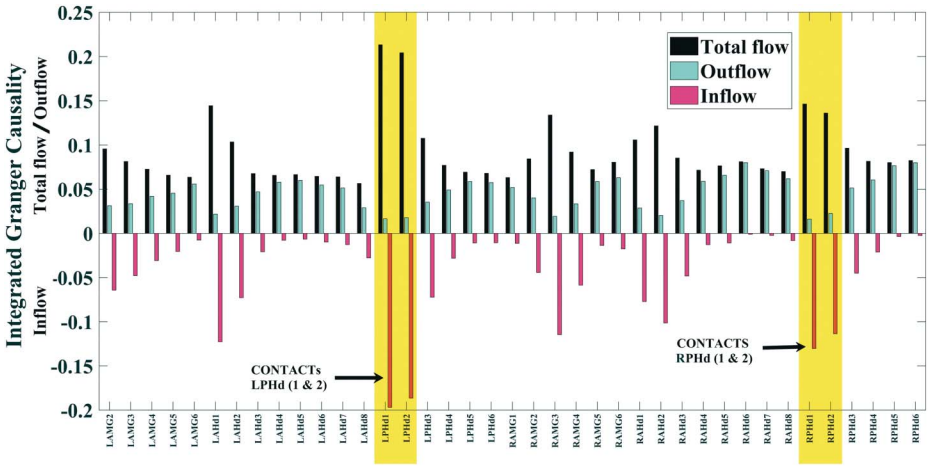

FIG. 3. Integrated Granger causality of high-frequency activities in the interictal state for patient C, showing the total causal flow, inflow, and outflow for all 39 valid recording contacts of the stereoEEG implant. Contacts LPHd1-2 and RPHd1-2 are the sites of independent bilateral visible seizure onsets and hold four of the top five ranks for both inflow and total causal flow.

8 of 12 conditions, including high, infraslow, preictal, and interictal phases of epilepsy. Total causal flow, dominated by inflow, matched the SOC in 7 of 12 conditions. These results suggest that both inflow and total causal flow might identify the SOZ during different phases of epilepsy for both high and infraslow frequency ranges, but the computation of total flow did not increase the yield compared with causal inflow alone. Nor did significant clusters of contacts around the SOC increase the total yield. As seen in Fig. 4, the detailed correspondence between the visual SOC and the sites of maximum causal inflow was also imperfect. Nearby contacts on the same electrode might have stronger inflow a centimeter away. This discrepancy could be because of limitations of visual identification, restricted spatial sampling, or simply stochastic variation.

DISCUSSION

The three patients reported here were selected specifically for the absence of anatomic lesions, to minimize the possibility that iEEG changes, including those at low frequencies, were related to the lesion rather than the epileptic focus alone. Some anatomic lesions, such as cortical dysplasias, are known to produce characteristic high-frequency ictal onset iEEG patterns.[9] Others, including tumors, produce prominent slow activity. It seemed possible that lesions that produce distinct patterns in the visual EEG might do so under quantitative and causal analysis as well.

These patients also had visible ictal onsets confined to SOC of one or two adjacent contacts; previous related series often defined a larger SOZ or irritable zone incorporating larger numbers of contacts. In the present, highly selective patient group, average follow-up is longer than in many larger series and the size of the invasive procedures is smaller. In particular, responsive neural stimulation and the simple implantation of electrodes are among the smallest focal interventions currently possible—even if inadvertent—and help to further ensure accurate identification of seizure origin. These characteristics lend confidence to our assessment that the SOZ had been accurately identified. In addition, one patient had recorded bitemporal posterior hippocampal seizure onsets. Patients with independent bitemporal seizure foci have not been described using similar techniques. In this case, the two recorded independent mirror hippocampal seizure onset channels both rank at the top by causal flow measures. The persistence of the epilepsy network seems unaffected by the type of cortex studied; similar results were found for primary motor area, cingulate gyrus, and hippocampus.

The universe of mathematical measures that have been applied to analysis of epilepsy networks is far greater than can be reviewed here. Techniques related to Granger causality include partial directed coherence[26,27] and the directed transfer function.[27] Betweenness centrality has been prominent among many candidate graph theory algorithms.[26] However, it did not improve on the yield of causal flow in the present small study or in further unpublished work. Yang and Madsen[28] reported that a wide range of algorithms derived from a somewhat different form of Granger analysis had for the most part similar yields across 25 surgical patients. In-degree performed best in that study; however, causal inflow was not compared. Computation of graph algorithms compliments but does not reflect more clearly the underlying physiology of the SOZ and its associated network.

One possible limitation to this study was the analysis of only one preictal segment and one interictal sample per patient. The number of EEG segments used for analysis varies widely across the relevant literature. There seems to be no consensus on the number of seizures to be analyzed per subject or on how to combine the results. As one of our selection criteria was that all seizures be visually identical, we analyzed only one specific segment per subject.

Under causal analysis, the epilepsy network is often dominant across all recording electrodes, with causal inflow at the seizure onset contacts, or at clusters of contacts involving it, ranking highest among more than 100 other recording sites. The minority of analyses that yielded less significant rankings are not necessarily devoid of localizing activity. Such activity might simply be less prominent, fluctuate over time and state, be potentially identifiable by a larger amount of data[26,28] or a different computational index,[28] or be revealed by cross-frequency correlations.[10] However, the purpose of this study was not to exhaust all possible calculations but to represent the epilepsy network as broadly as possibly using a single, relatively straightforward measure.

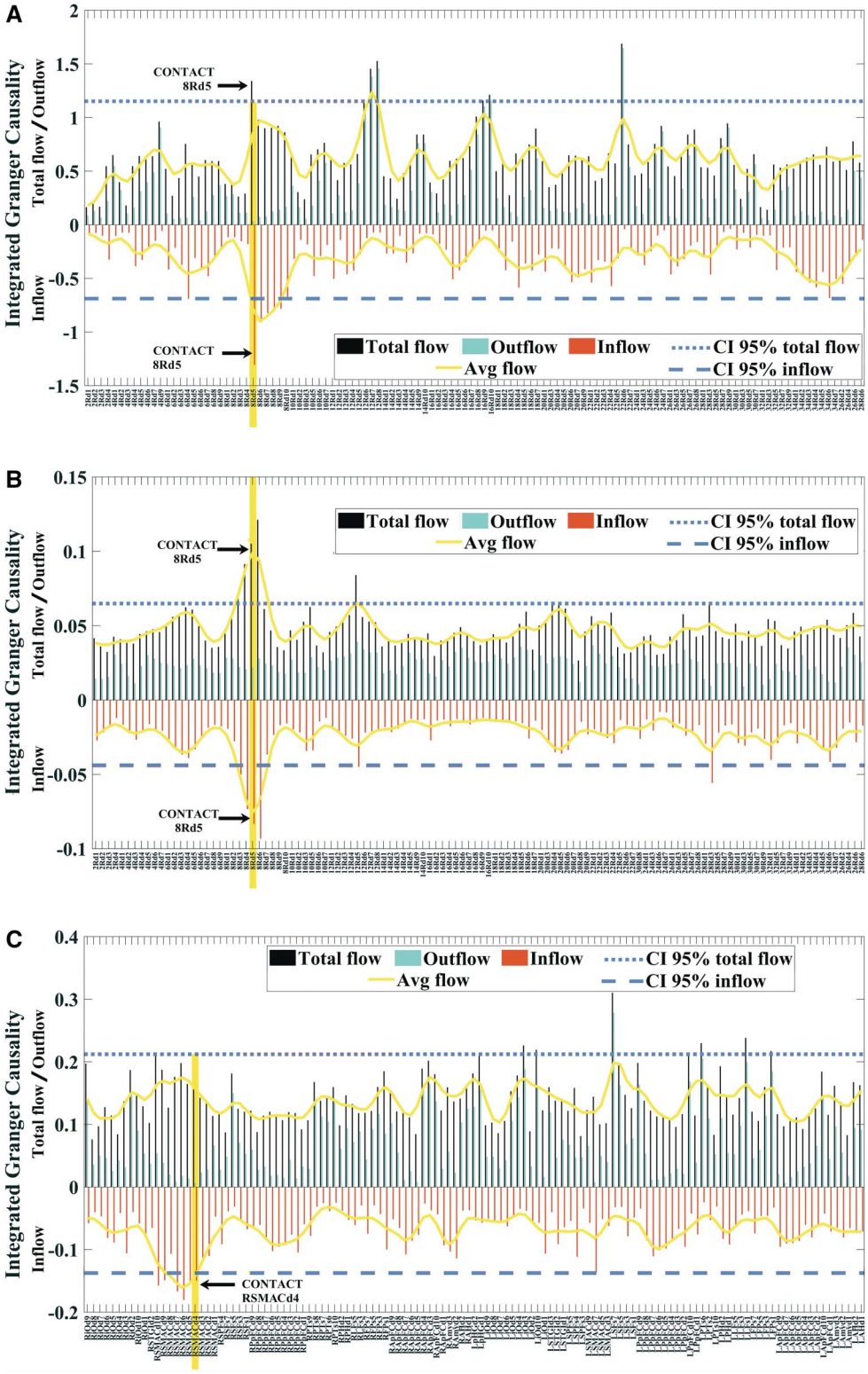

FIG. 4. **A**, Integrated Granger causality of infraslow activities in the interictal state for patient A, showing total causal flow, inflow, and outflow for all 118 valid recording contacts of the stereoEEG implant. Contact 8Rd5 in motor cortex is the site of visible seizure onset and has the strongest causal inflow of all contacts across the entire implant. Yellow outlines represent the group average values of flow clusters across inflow and total flow. Cyan dashed and dotted lines represent the 95% confidence intervals for random clusters of channels determined by jackknife substitution. The inflow cluster including 8Rd5 exceeds the 95% confidence limit on causal inflow and total flow and is the most significant cluster overall. **B**, Integrated Granger causality of high-frequency activities in the preictal state for patient A. Contacts, labels, colored outlines, and boundaries as in (**A**). For contact 8Rd5, both inflow and total flow exceed all but one contact immediately adjacent to it. The cluster of five adjacent contacts including 8Rd5 also exceeds the 95% confidence limits on causal flow and is the most significant cluster overall. **C**, Integrated Granger causality of infraslow frequency activities in the preictal state for patient B. Total causal flow, inflow, and outflow for all 123 valid recording contacts of the stereoEEG implant. Contact RSMAcd4 in cingulate gyrus is the site of visible seizure onset, ranking 5th of 123 for causal inflow but outranked only by nearby contacts on the same electrode. The cluster of neighboring contacts including RSMACd4 exceeds the 95% confidence limit on causal inflow and is the most significant cluster overall.

Surround inhibition near the SOZ was described many years ago by Prince and Wilder.[29] An inhibitory ictal penumbra was further defined by Schevon et al[30] in the present era. More recently, findings analogous to our own have been described for the preictal period using the graph theory measure in-degree[28] and for the interictal period using a number of measures, especially partial

TABLE 1. Granger Causality Measures Identifying the Seizure Onset Channels

	High Frequency		Infraslow Frequency	
Measure	**Preictal**	**Interictal**	**Preictal**	**Interictal**
Total flow	3	2	0	2
Inflow	3	1	2	2

Conditions for which corresponding causal measures localized the seizure onset contacts across preictal and interictal periods at ripple and infraslow frequencies.

directed coherence at alpha frequencies.[27] Our causal flow data consolidates and extends the findings that inhibition is ubiquitous across different phases of epilepsy and extends from ripple to infraslow frequencies. Further, as illustrated in Figs. 3 and 4, prominent inflow activity can be detected for distances up to 2 cm along the electrode, reaching a maximum near the seizure onset contacts and diminishing with distance on one or both sides.

The present results support the existence of a widespread, stable iEEG network, salient at both very high and very low frequencies through different phases of focal epilepsy, from interictal to preictal, and extending close to the edge of the visible seizure onset. Incorporating the causal analysis of classic infraslow frequencies from 0.01 to 0.1 Hz, they demonstrate that the latter carry localizing information comparable with that of the higher frequency bands. Under all these conditions, a single measure of inward causal flow characterizes the region of seizure onset. Within the limits of the present analysis, the SOZ seems never to be identified by prominent causal source activity. The macroscopic spatial extent of ongoing inhibition suggests that it involves a considerable area surrounding the SOC and might be one mechanism by which epilepsy affects the function and even the structure of nearby regions during long intervals when no seizure activity is apparent. Additionally, the directionality of this effect suggests an interesting possibility: that the sources of inhibition might themselves be relatively overactive and that this, rather than activity originating in the SOZ, could be responsible for some effects of epilepsy on more remote portions of the network. Even as the evidence for the epilepsy network strengthens, its underlying features may hold further surprises.

ACKNOWLEDGMENTS

The authors thank Bhim Mani Adhikari for suggestions regarding data analysis.

REFERENCES

1. da Silva FL, Pijn JP, Boeijinga P. Interdependence of EEG signals: linear vs. nonlinear associations and the significance of time delays and phase shifts. Brain Topogr 1989;2:9–18.
2. Kini LG, Bernabei JM, Mikhail F, et al. Virtual resection predicts surgical outcome for drug-resistant epilepsy. Brain 2019;142:3892–3905.
3. Müller M, Caporro M, Gast H, et al. Linear and nonlinear interrelations show fundamentally distinct network structure in preictal intracranial EEG of epilepsy patients. Hum Brain Mapp 2020;41:467–483.
4. Epstein CM, Adhikari BM, Gross R, Willie J, Dhamala M. Application of high-frequency Granger causality to analysis of epileptic seizures and surgical decision making. Epilepsia 2014;55:2038–2047.
5. Modur PN, Vitaz TW, Zhang S. Seizure localization using broadband EEG: comparison of conventional frequency activity, high frequency oscillations and infraslow activity. J Clin Neurophysiol 2012;29:309.
6. Wu S, Veedu HP, Lhatoo SD, Koubeissi MZ, Miller JP, Lüders HO. Role of ictal baseline shifts and ictal high-frequency oscillations in stereo-electroencephalography analysis of mesial temporal lobe seizures. Epilepsia 2014;55:690–698.
7. Thompson SA , Krishnan B, Gonzalez-Martinez J, et al. Interictal infraslow activity in stereoelectroencephalography: from focus to network. J Clin Neurophysiol 2016;33:141–148.
8. Inoue T, Morito I, Masao M, et al. Interictal slow and high-frequency oscillations: is it an epileptic slow or red slow? J Clin Neurophysiol 2019;36:166–170.
9. Janca R, Jahodova A, Hlinka J, et al. Ictal gamma-band interactions localize ictogenic nodes of the epileptic network in focal cortical dysplasia. Clin Neurophysiol 2021;132:1927–1936.
10. Hashimoto H, Khoo HM, Yanagisawa T, et al. Phase-amplitude coupling of ripple activities during seizure evolution with theta phase. Clin Neurophysiol 2021;132:1243–1253.
11. Granger CW. Investigating causal relations by econometric models and cross-spectral methods. Econometrica 1969;37:424–438.
12. Adhikari BM, Epstein CM, Dhamala M. Localizing epileptic seizure onsets with Granger causality. Phys Rev E Stat Nonlin Soft Matter Phys 2013;88:030701.
13. Coben R, Mohammad-Rezazadeh I. Neural connectivity in epilepsy as measured by granger causality. Front Hum Neurosci 2015;9:194.
14. Coito A, Plomp G, Genetti M, et al. Dynamic directed interictal connectivity in left and right temporal lobe epilepsy. Epilepsia 2015;56:207–217.
15. Park EH, Madsen JR. Granger causality analysis of interictal iEEG predicts seizure focus and ultimate resection. Neurosurgery 2018;82:99–109.
16. Andrzejak RG, David O, Gnatkovsky V, et al. Localization of epileptogenic zone on pre-surgical intracranial EEG recordings: toward a validation of quantitative signal analysis approaches. Brain Topogr 2015;28:832–837.
17. Grinenko O, Li J, Mosher JC, et al. A fingerprint of the epileptogenic zone in human epilepsies. Brain 2018;141:117–131.
18. Gnatkovsky V, Pelliccia V, de Curtis M, Tassi L. Two main focal seizure patterns revealed by intracerebral electroencephalographic biomarker analysis. Epilepsia 2019;60:96–106.
19. Katariwala N, Bakay RA, Pennell PB, Olson LD, Henry TR, Epstein CM. Remission of intractable partial epilepsy following implantation of intracranial electrodes. Neurology 2001;57:1505–1507.
20. Schulze-Bonhage A, Dennig D, Wagner K, et al. Seizure control resulting from intrahippocampal depth electrode insertion. J Neurol Neurosurg Psychiatry 2010;81:352–353.
21. Roth J, Olasunkanmi A, Ma TS, et al. Epilepsy control following intracranial monitoring without resection in young children. Epilepsia 2012;53:334–341.
22. Delorme A, Makeig S. EEGLAB: an open source toolbox for analysis of single-trial EEG dynamics including independent component analysis. J Neurosci Methods 2004;134:9–21.
23. Dhamala M, Rangarajan G, Ding M. Estimating Granger causality from Fourier and wavelet transforms of time series data. Phys Rev Lett 2008;100:018701.
24. Dhamala M, Rangarajan G , Ding M. Analyzing information flow in brain networks with nonparametric Granger causality. Neuroimage 2008;41:354–362.
25. Miller RG. The jackknife-a review. Biometrika 1974;61:1–15.
26. Li YH, Ye XL, Liu QQ, et al. Localization of epileptogenic zone based on graph analysis of stereo-EEG. Epilepsy Res 2016;128:149–157.
27. Narasimhan S, Kundassery KB, Gupta K, et al. Seizure-onset regions demonstrate high inward directed connectivity during resting-state: an SEEG study in focal epilepsy. Epilepsia 2020;61:2534–2544.
28. Yang VB, Madsen JR. Extensions of granger causality calculations on brain networks for efficient and accurate seizure focus identification via iEEGs. Brain Sci 2021;11:1167.
29. Prince DA, Wilder BJ. Control mechanisms in cortical epileptogenic foci*: surround inhibition. Arch Neurol 1967;16:194–202.
30. Schevon CA, Weiss SA, McKhann G Jr, et al. Evidence of an inhibitory restraint of seizure activity in humans. Nat Commun 2012;3:1–11.